Journal of Materials Chemistry A

Localized High Concentration Electrolyte Behavior near a Lithium-Metal Anode Surface

Journal:	*Journal of Materials Chemistry A*
Manuscript ID	TA-ART-08-2019-008935.R2
Article Type:	Paper
Date Submitted by the Author:	11-Oct-2019
Complete List of Authors:	Zheng, Yu; Texas AandM University, Chemical Engineering Soto, Fernando; Texas A&M University, Chemical Engineering Ponce, Victor; Texas A&M University, Chemical Engineering Seminario, Jorge; Texas A&M University College Station, Cao, Xia; Pacific Northwest National Laboratory, Energy and Environment Directorate Zhang, Ji-Guang; Pacific Northwest National Laboratory, Balbuena, Perla; Texas AandM University, Chemical Engineering

Localized High Concentration Electrolyte Behavior near a Lithium-Metal Anode Surface

Yu Zheng[1,3], Fernando A. Soto[1], Victor Ponce[1,2], Jorge M. Seminario[1,2,4], Xia Cao[5], Ji-Guang Zhang[5], and Perla B. Balbuena[1,2,3,*]

[1]Department of Chemical Engineering, [2]Department of Materials Science and Engineering, and [3]Department of Chemistry, [4]Department of Electrical Engineering, Texas A&M University, College Station, Texas 77843, United States; [5]Energy and Environment Directorate, Pacific Northwest National Laboratory, Richland, Washington 99354, United States

*e-mail: balbuena@tamu.edu

Abstract

Wide-scale practical application of rechargeable lithium-metal batteries remains a significant challenge due to dendrite growth. To overcome this challenge, electrolytes must be designed to allow for the formation of protective solid electrolyte interphase (SEI) layers on the highly reactive lithium-metal anode (LMA) surfaces. Recently, novel localized high-concentration electrolytes (LHCEs) were introduced as a potential solution to enable dendrite-free cycling of LMAs, by using an inert solvent to "dilute" the high concentration electrolytes. Ideally, the diluent itself does not dissolve the salt but is miscible with the solvent to form a localized high concentrated salt/solvent cluster surrounded by the diluent. However, detailed structure and potential surface reactions that may take place in LHCE environment are not yet clear. In this work, we investigated the reactivity of a 1M lithium bis(fluorosulfonyl)imide (LiFSI) in a mixture of dimethoxyethane (DME)/Tris(2,2,2-trifluoroethyl)orthoformate (TFEO) (1:3 by mol) electrolyte near a Li metal surface based on density functional theory and *ab-initio* molecular dynamics (MD) simulations. Selected liquid interfacial configurations were obtained from classical MD simulations. Our results indicate that when salt and TFEO molecules are close to each other and to the surface, fluorine anions resulting from the fast salt anion decomposition can trigger a cascade of reactions that lead to the decomposition of TFEO. However, if the Li cation is initially solvated by DME and the anion forming a complex, the stability of the anion increases significantly. The Li solvated structure is implied in the LHCE concept; however statistically the larger amount of TFEO molecules suggest also the first scenario leading to TFEO decomposition. Therefore, the broader implication of our simulations is that the defluorination of TFEO may contribute, together with the anion decomposition, to the observed rapid formation of a stable SEI on the surface of the lithium metal; consequently, favorably affecting the stability of LMAs during battery operation.

Keywords: lithium-ion batteries, lithium metal anodes, dendrite formation, localized high-concentration electrolytes, *ab-initio* molecular dynamics

Introduction

Because lithium (Li) metal has the highest specific capacity (3,860 mAh/g) and lowest negative electrochemical potential (-3.04 V vs. standard hydrogen electrode), Li-metal batteries (LMBs) have become the most promising next-generation energy storage systems [1-6]. However, conventional LMBs exhibit low Coulombic efficiency (CE) and safety concerns. For instance, commercial electrolytes typically consisting of 1–1.2 M lithium hexafluorophosphate ($LiPF_6$) in a mixture of carbonate solvents will lead to dendrite formation during repeated charge/discharge processes [7-9]. Strategies to prevent dendrite formation include improving the stability of the solid electrolyte interphase (SEI) layer or using mechanical barriers to achieve smooth Li^+ deposition and suppress dendrite penetration [10,11]. As an alternative, various high-concentration electrolytes (HCEs) (e.g.,> 3 M) with unique solvation structure and ion transport mechanisms have been successfully developed to suppress the dendritic Li growth [12,13]. For example, Zhang *et al*. [14] reported that the use of 4 M lithium bis(fluorosulfonyl)imide (LiFSI) in 1,2-dimethoxyethane (DME) could improve the CE of LMAs to 99.2% while also eliminating dendrite growth. However, the usage of a large amount of expensive lithium salt in the HCE systems also leads to several disadvantages, including low conductivity and high viscosity [15].

One solution to resolve these issues without losing the unique characteristics of HCEs could be introducing an inert co-solvent to dilute the concentrated electrolyte resulting in localized high-concentration electrolytes (LHCEs) [16]. The choice of the co-solvent in LHCEs is critical for the performance of LMBs. Ideally, the diluent should have appropriate coordination property that enables a high solubility of HCE while maintaining the Li^+ solvation structure. Bis(2,2,2-trifluoroethyl) ether (BTFE), a hydrofluoroether that meets the major requirements, was employed by Zhang and co-workers as the diluent in an HCE consisting of 5.5 M LiFSI/dimethyl carbonate (DMC) [17]. This LHCE enabled dendrite-free cycling of LMAs with high CE (99.5%) and excellent capacity retention (>80% after 700 cycles). Furthermore, the choice of the inert diluent is critical when considering the formation of a SEI layer, which can significantly affect the performance of the battery [18]. As the analogous to BTFE, tris(2,2,2-trifluoroethyl)orthoformate (TFEO) with a higher fluorination degree was recently identified to be suitable for diluting ether-based HCE

systems.[19] The interesting and detailed study by Zhang et al.[19] describes the formation of a monolithic mostly inorganic amorphous film able to exert a substantially improved LMA performance. Moreover, this TFEO-based LHCE electrolyte was shown[19] to be effective also at the cathode side forming a cathode-electrolyte interface that protects the structure of the metal oxide cathodes. However, the mechanism by which the electrolyte solution enhances the stability of the Li metal is still unknown. For instance, the initial stages of electrolyte decomposition and nucleation and growth of the SEI layer, remain unclear. Recent studies suggest that the decomposition of the fluorinated non-aqueous solvents lead to the formation of lithium fluoride (LiF) layer on the surface of the Li metal, but a mechanistic explanation is missing[20]. Other experimental work related to LHCEs, attributed LiF formation to the decomposition of the Li-salt anion.[21]

Over the last decades, computational modeling on energy materials is an additional tool that helps understanding and designing the properties of battery materials and operation.[22-24] For example, electronic structure and dynamics models based on DFT provide convenient tools to analyze physical, chemical, and reactivity properties of electrolyte materials.[25,26] Atomistic scale simulations such as classical molecular dynamics add fundamental insights into structure and dynamics of electrolyte materials.[27-30] In addition, due to the complexity of materials and processes, computational methods that combine at least two modeling approaches are frequently needed. In this work, we present a theoretical first-principles study on the reactivity of the LHCE system composed of 1M LiFSI/DME+TFEO (1:1:3 by mol) [19] in contact with the (100) facet of a Li metal slab to address these outstanding questions: How is the monolithic SEI formed? What are the mechanisms by which LHCEs enable stability of electrolyte with the Li metal slab?

Methodology

First-principles calculations were performed using the Perdew−Burke−Ernzerhof (PBE) exchange-correlation functional within the generalized-gradient approximation (GGA) to density functional theory as implemented in the Vienna *Ab-Initio* Simulation Package (VASP) electronic structure code [31,32]. We used a plane-wave basis set in conjunction with project augmented wavefunctions (PAW) [33]. Gaussian smearing with a width of 0.05 eV was utilized to set the partial occupancies to each wave function. We used a 2×2×1 k-point mesh and a 400 eV kinetic energy cutoff. *Ab-initio* molecular dynamics (AIMD) simulations were run at 330 K with a 1 fs time step

within the NVT ensemble. Tritium masses were replaced for protons to allow a time step of 1 fs with a Nose-mass parameter of 0.5 to control the temperature oscillations. Trajectories were recorded at every step, and the Bader charges as implemented by Henkelman *et al.*[34,35] were used to compute the atomic partial charges. We note that although our AIMD runs were about 20 ps long, we were able to study the initial reactivity of the systems, at least for the fastest anion and TFEO decomposition reactions. A 9-layer (3 × 3) supercell model with the middle three layers fixed was employed to represent the LMA surface. In a previous computational work [36] where the Li metal slab served as the anode electrode, we analyzed the stability of the (100), (110), and (111) facets given by their surface energy, defined as the excess energy per unit area of a particular facet. This study revealed that the (100) facet is the most thermodynamically stable. For this reason the (100) facet was used in this study. Due to the volume of the simulation cell, one salt molecule was required to achieve the 1 M salt concentration. Optimized structures for DME and LiFSI were taken from our previous work [37]. The TFEO molecule was optimized the Gaussian 09 (G09) package with a hybrid functional B3LYP and the 6-311+G(d,p) basis set [38,39].

Classical molecular dynamics (CMD) simulations were carried out to elucidate the structure of the bulk electrolyte. A box of dimensions 37 Å x 37 x Å 37 x Å was used to hold 30 LiFSI, 48 DME, and 120 TFEO molecules representing a 1M LiFSI/DME/TFEO solution . The molecules were initially randomly distributed, and two different configurations were tested: one where all the LiFSI molecules were initially associated and the other where all of them were initially dissociated. The box was initially equilibrated at 5K during 1ns, and then heated for another nanosecond from 5 to 300K (rate of 0.3 $x10^{-3}$ K/ps) in the NPT ensemble. The equilibration and heating periods were followed by another equilibration at 300 K (1 ns) and a production period of 9 ns. The temperature was kept constant using the Nose-Hoover thermostat in the NPT ensemble and 50 fs as dumping parameter. The force fields used in these simulations were the Class 2[40,41] and Lennard Jones[41,42] for all atoms.

The reduction potentials were calculated based on the following thermodynamic cycle:

$$\begin{array}{ccc} M(g) + e^- & \xrightarrow{\Delta G_{red}(g)} & M^-(g) \\ \uparrow -\Delta G_{sol}(M) & & \downarrow \Delta G_{sol}(M^-) \\ M(sol) + e^- & \xrightarrow[\Delta G_{red}(sol)]{} & M^-(sol) \end{array}$$

where *M* and e^- represent a solvated molecule and an electron, respectively. Then, the reduction potential in the Li/Li^+ scale results from the following equation, where F is the Faraday constant:

$$E_{red}(\text{vs. Li/Li}^+) = -\Delta G_{red}(\text{sol})/F - 1.37\ \text{V} = -[\ \Delta G_{red}(\text{g}) + \Delta G_{sol}(M^-) - \Delta G_{sol}(M)]/F - 1.37\ \text{V}.$$

Reduction potentials for various conformations were calculated with the B3LYP hybrid functional and the 6-311+G(p,d) basis set as implemented in the G09 program. The solvation effects were represented by the polarizable continuum model (PCM) with tetrahydrofuran (THF) as a solvent.[43]

Results and Discussion

Liquid structure. The structural analysis was done by evaluating the radial distribution functions. The most important features are the following: The three components have LiO interactions with the three species (TFEO, FSI, and DME, see Figure 1) that compete with each other. However, the strongest interactions are Li-O where the Li cations interact with O of the DME or with O of the anion. Li-O interactions from cation-TFEO are also present but they are found to be weaker.

Table 1. Peak location (Å), intensity = ratio of local density to bulk density (in parenthesis), and 1st shell average coordination number (in square brackets)

Initial configuration	Li-O (FSI)	Li-O (DME)	Li-O (TFEO)
Undissociated salt	2.19 (80.9) [1.6]	2.29 (29.6) [0.7]	2.32 (2.85) [0.8]
Dissociated salt	2.20 (49.4) [1.2]	2.29 (20.59) [0.6]	2.58 (5.06) [1.5]

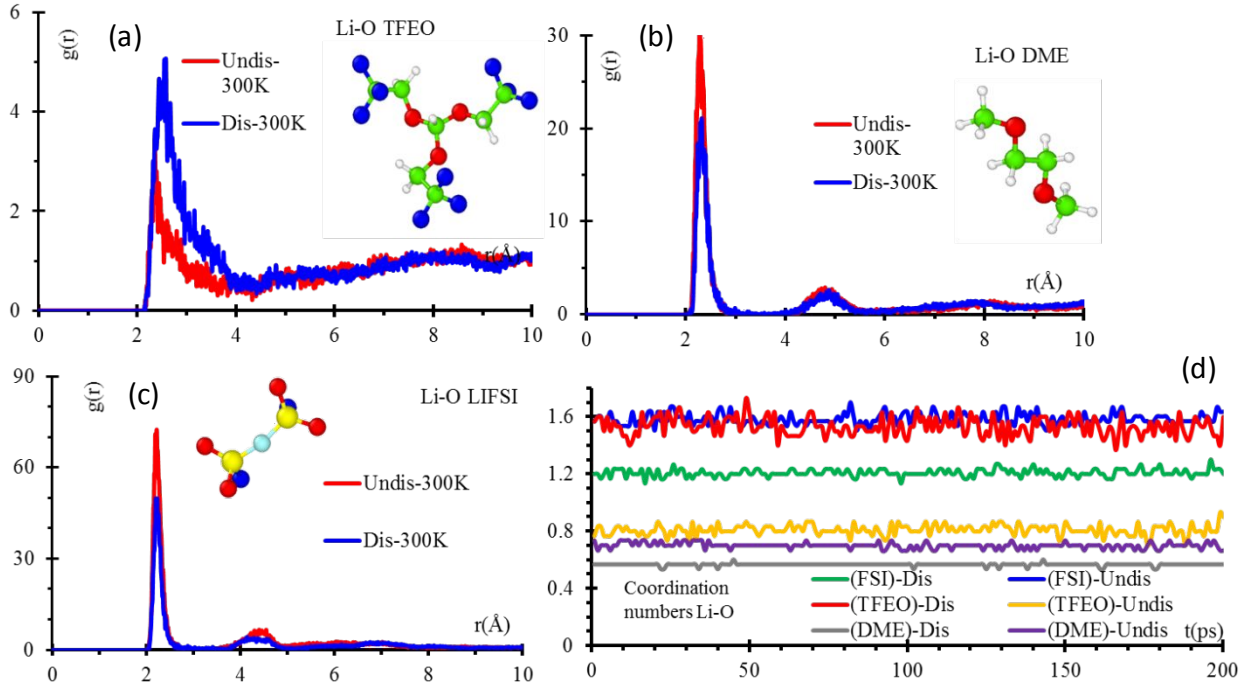

Figure 1. Li-O radial distribution functions between Li ions and a) TFEO, b) DME, and c) FSI. d) Time evolution (in ps) of the 1st shell average coordination numbers for Li atoms corresponding to two initial configurations (see text).

Table 1 reveals that for the initial configuration having undissociated salt molecules, the Li cation interacts strongly with its FSI anion (Fig. 1c), but also with TFEO molecules and in the same extent with DME molecules, as indicated by their 1st shell average coordination numbers. However, the Li-O interactions with DME (Fig. 1b) are sharper than the ones with TFEO (Fig. 1a) showing broader peaks characteristic of wider range of interaction distances. On the other hand, initial configurations having all dissociated salt molecules show a slightly lower cation-anion coordination number, and higher number of interactions with TFEO. Moreover, when the salt molecules are initially dissociated, the strongest interaction is with the DME molecules (Fig. 1b), although interactions with FSI and TFEO are also detected. In a random solution, we expect to have some contributions from both limiting cases. Therefore, a dominance of Li-FSI followed by Li-DME interactions, and lastly (but not negligible) Li-TFEO interactions.

In summary, although the three electrolyte components (anion, TFEO, and DME) have LiO interactions that compete with each other (Figure 1), the simulations reveal much stronger interactions of the Li cation with its FSI anion and with DME respectively, while the more abundant TFEO is always surrounding these complexes. Because of the larger proportion of TFEO,

statistically there are cases where DME is not interacting with Li, thus the TFEO molecules continuously surrounding the ion pair may play a role. Also, because of the relatively small amount of the DME solvent, the salt tends to remain associated.

Structure and dynamics of the electrolyte at the Li surface. Based on the bulk structural results, two initial configurations for the LiFSI salt were used for the AIMD simulations of the electrolyte in contact with the Li surface.

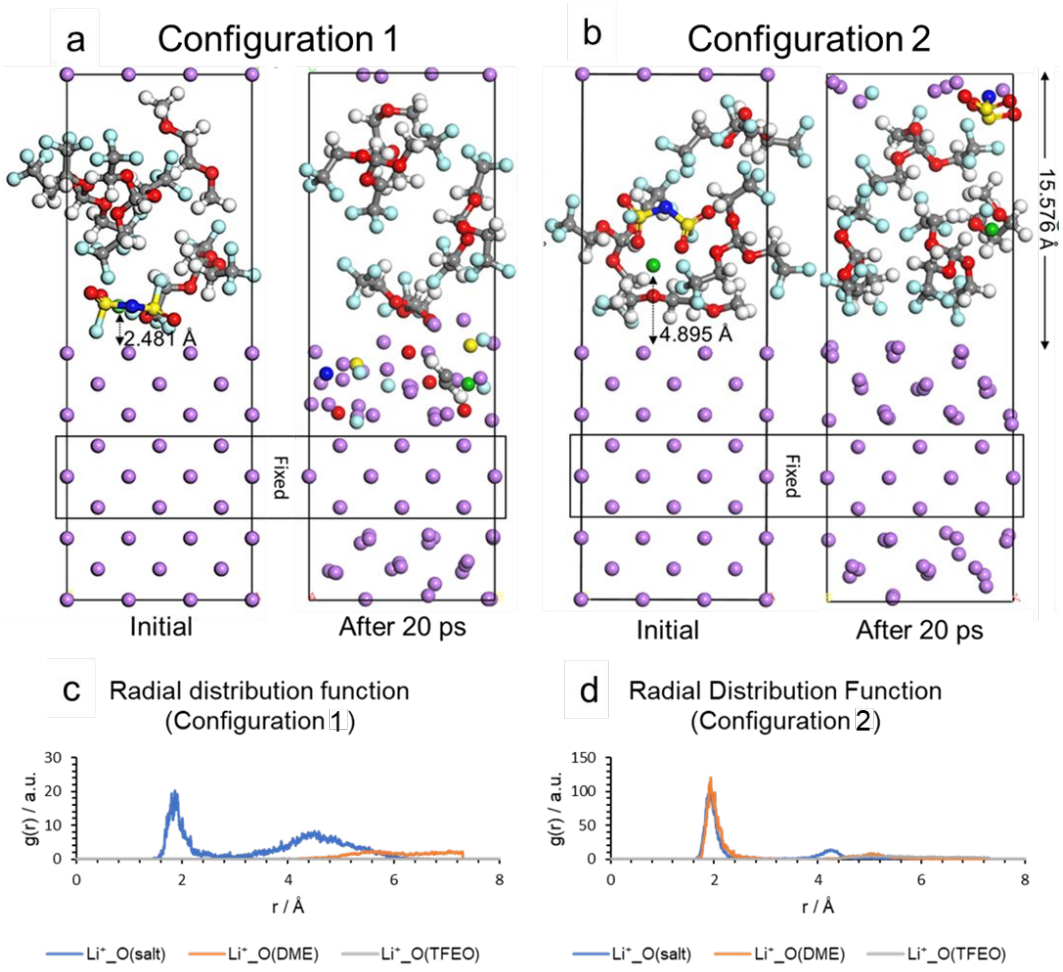

Figure 2. Initial and final (after 20 ps) snapshots of lithium−metal anode surface and 1 M LiFSI/DME/TFEO electrolyte in AIMD simulation. (a) Configuration 1 (salt molecule relatively separated from DME) and (b) Configuration 2 (Li cation is solvated by both anion and DME). Color code: lithium from the slab (salt), purple (green); oxygen, red; carbon, gray; fluorine, light blue; sulfur, yellow, nitrogen, blue; hydrogen, white. Radial distribution function of (c) configuration 1 and (d) configuration 2 from AIMD simulations. Color code: Li^+_O (salt), blue; Li^+_O (DME), orange; Li^+_O (TFEO), gray.

They represent the two limiting situations where the LiFSI salt molecule may be located relatively far or close to the DME solvent molecule. In the first case, TFEO molecules may be close to the salt molecule. Figure 2 (a) and (b) show the initial and final snapshots of these two systems. For Configuration 1, the LiFSI salt is initially located approximately 2.5 Å away from the surface of the Li metal slab and is surrounded by TFEO molecules, but relatively far from DME. For Configuration 2, the LiFSI salt is initially situated about 4.9 Å away from the anode's surface and the cation is solvated both by the anion and by the DME molecule. To better illustrate the structure of the electrolytes under these two different configurations, the radial distribution functions (RDFs) for Li^+-O (O, salt; O, DME; O, TFEO) pair interactions were evaluated over the entire trajectory of the 20 ps AIMD simulation run. As shown in Figure 2 (d), the first solvation shell of Li^+ in Configuration 2 is well defined by oxygen atoms from both FSI^- and DME at 1.9~2.0 Å, indicating that Li^+ has a relatively strong interaction with O (FSI^-), as well as with the DME molecule. This is in a good agreement with the assumption of LHCEs in which the salt anions would enter the solvation shell of solvent/diluent to form contact ion pairs (CIPs)[12]. The dilution strategy introduces an inert diluent molecule that does not change the local coordination environment of the concentrated electrolytes; therefore the CIPs structures can be maintained. This analysis is in agreement with that of the Raman spectra for electrolytes with different salt concentrations in pure DMC and DMC/BTFE mixtures.[9] With increasing LiFSI salt concentration up to 5.5 M in pure DMC, the free DMC ($O–CH_3$ stretching vibration band at ≈920 cm^{-1}) gradually diminishes to form Li^+-coordinated DMC (≈940 cm^{-1}). Adding BTFE as a diluent, the Li^+-coordinated DMC solvation structure is well preserved and the vibrational band of BTFE at 830–840 cm^{-1} does not change in different LiFSI/DMC-BTFE solutions. [9]

In contrast, for Configuration 1, shown in Figure 2 (c), the first solvation shell is only consisting of the oxygen atoms from FSI^- facing towards the cation at 1.9~2.0 Å, and the second solvation shell is defined by the oxygen atoms from FSI^- but facing opposite to the cation. Thus**,** the interaction between the salt and solvent with the diluent molecules is quite weak. Also, RDFs (Figure S1) for hydrogen atoms in DME and oxygen/fluorine atoms in TFEO demonstrate sufficient inertness of the diluents. Van der Waals interactions between TFEO and DME should be responsible for the dissolution of concentrated electrolytes [44].

In Configuration 1, the FSI anion undergoes an immediate decomposition (Figure S2). The anion decomposition (within the first 30 fs of simulation time) proceeds through the simultaneous elongation of the anion's N-S and S-F bonds. This initial decomposition reaction triggers a cascade of decomposition reactions that results in the complete dissociation of all the anion's bonds within 4.5 ps of simulation time. The decomposition products (e.g., F^-, NSO_2^{-2} and SO_2^{-2}) move within the interface region with one F^- anion moving closer to the Li slab and the other F^- anion moving to the vicinity of the nearby TFEO molecule. The SO_2^{-2} anion undergoes complete dissociation with the sequential release of its O atoms within 2 ps of simulation time. Meanwhile, the decomposition of the NSO_2^{-2} anion is slightly slower and after 2 ps of simulation time a N-S bond remains at the interface region. After 4.5 ps of simulation time, this N-S bond disappears leading to N^{-2} and S^{-2} anion species interacting with Li^+ at the interface region.

Interestingly, the F anion found closer to the TFEO molecule serves as a trigger to initiate the sequential defluorination and decomposition of TFEO molecules in Configuration 1. The sequential decomposition mechanism of one of the three TFEO molecules is illustrated in Figure 3. Under the attack of an F anion derived from the decomposition of the LiFSI salt, there is a dynamic H-F bond formed at 200 fs, accompanied by the cleavage of C-F bond to lose one F atom. After a few hundred femtoseconds, the remaining TFEO fragment gains one more electron from the Li surface to defluorinate again. The H atom extracted by the F anion when HF molecule forms would migrate close to the terminal C atom, meanwhile the third F atom also gets detached. After the TFEO molecule gets 4 electrons in total, a C-O bond breaks to form a C_2H_2 molecule. The total reaction of TFEO decomposition can be summarized as:

$$TFEO + 4e^- \rightarrow C_2H_2 + 3F^- + CHO(OCH_2CF_3)_2^- \qquad (1)$$

The reaction energy was calculated to be ΔE (0 K) = -292.10 kcal/mol, which indicates this TFEO decomposition mechanism is thermodynamically favorable. The instability of TFEO in contact with Li ions was also verified by calculation of the reduction potential of the complex TFEO/Li^+ (Figure 3) where a C-O bond of the TFEO molecule is broken in the reduced state. This indicates that the decomposition of TFEO is a synergistic reaction facilitated by Li^+ because the reduced anion (from TFEO) can be stabilized by the Li cation. These observations agree with our reduction

potential calculations, where we found that an isolated LiFSI salt has a highly positive reduction potential of 2.35 V, while the calculated reduction potentials of isolated DME and TFEO are -1.33 V and - 0.81 V, respectively. Therefore, in this LiFSI/DME/TFEO electrolyte solution, due to the charge transferred from the Li metal slab to the electrolyte solution, the LiFSI salt should get reduced most easily while reduction of DME should be the hardest. It is also noteworthy that no decomposition of DME molecules was observed during the entire 20 ps of AIMD simulation time in any of the three configurations, indicating the superior stability of the DME solvent in this electrolyte solution.

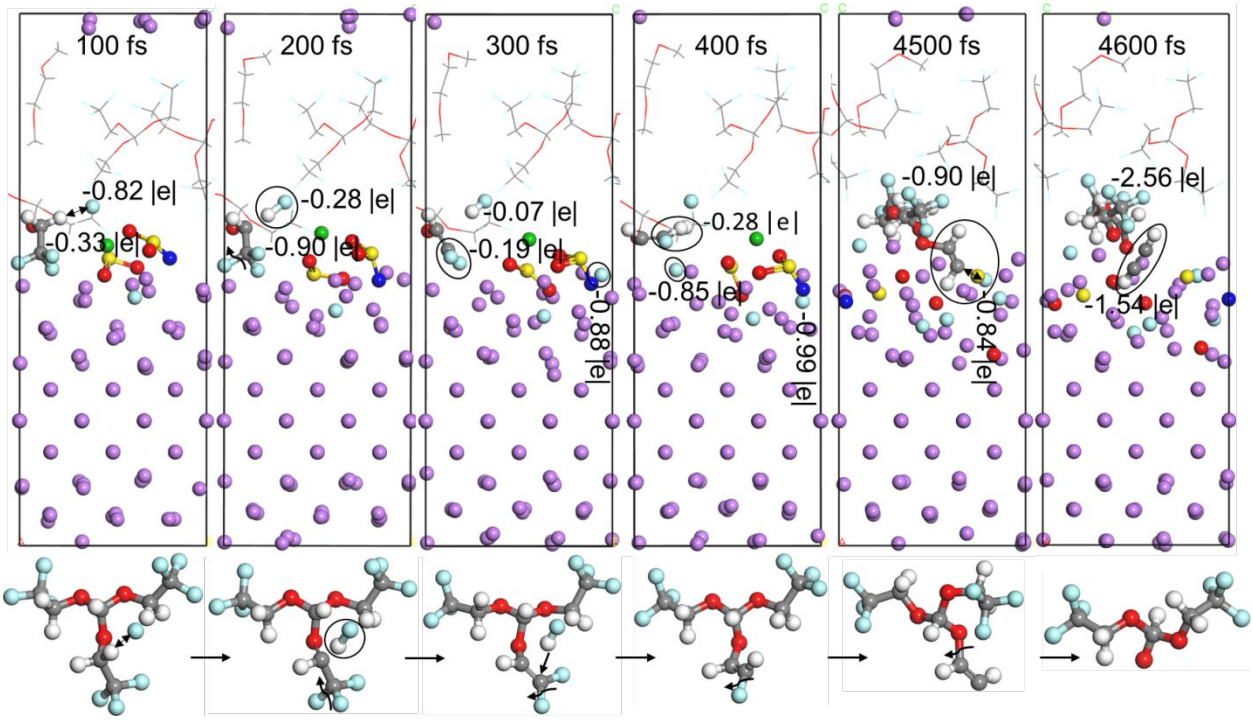

Figure 3. Snapshots showing the time evolution of the decomposition of the TFEO molecule in Configuration 1. Color code as in Figure 1.

On the other hand, no decomposition of the TFEO molecule was observed in Configuration 2, where the LiFSI salt molecule strongly interacts with the DME solvent molecule. The stability of LiFSI in this CIPs solvent structure is comparatively increased. The LiFSI molecule does not undergo any bond breakage during the first 10 ps until it obtained enough negative charge transferred from the Li metal slab. At this time, the salt molecule gets reduced in just 1ps losing its two terminal F atoms, and the remaining $N(SO_2)_2^{3-}$ fragment keeps stable till the end of

simulation (shown in Figure S3). Calculated reduction potentials (Table 2) for both isolated molecules and complexes with other electrolyte species of this LHCE system reveal that the fast TFEO decomposition discussed for Configuration 1 is in agreement with reduction potentials calculated for the TFEO/Li^+ complex shown in Figure 3. As illustrated in the reduced state of TFEO, Li^+ is located more closely to O8 (-0.57 e) to form a Li-$CHO(OCH_2CF_3)_2$ complex. The calculated reduction potentials for both isolated molecules and complexes with other electrolyte species are summarized in Table 2. When Li^+ is coordinated to the O atoms of TFEO, the calculated reduction potential of the TFEO/Li^+ complex is 2.52 V, which is higher by 3.33 V than that of the isolated molecule. The stability of DME can also be explained by its reduction potential values. Unlike TFEO, even if the DME molecule interacts with Li^+, FSI^-, or LiFSI, the calculated spin density (an indicator of the localization of the electron) is never located on the DME molecule. Therefore, no reduction of DME can be observed in any of the three configurations until the appropriate electrode potential allows the needed electron transfer.[45] This analysis gives us a hint that the structure of the solution defines specific orientations of LiFSI that in turn may play an important role in facilitating the decomposition of the TFEO molecule when this molecule is close to the surface.

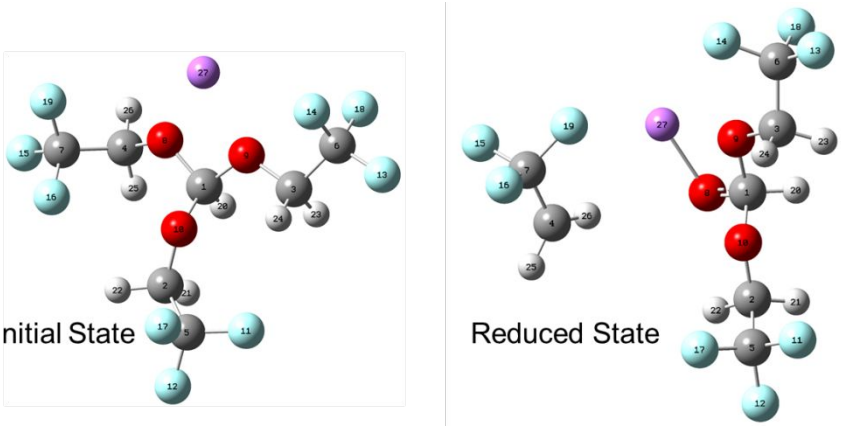

Figure 4. Initial state and final state of the TFEO/Li^+ complex. Color code as in Figure 1.

Table 2. Reduction potentials for isolated molecules and complexes with other electrolyte species. All values are given in V. A value of 1.37 V was subtracted to convert the potentials into the Li/Li^+ scale. Initial state and reduced state configurations for each system are shown in Figure S4.

Isolated Molecule			**with Li^+**		**with FSI^-**		**with LiFSI**	
DME	**TFEO**	**LiFSI**	**DME**	**TFEO**	**DME**	**TFEO**	**DME**	**TFEO**
-1.33	**-0.81**	**2.35**	**0.11**	**2.52**	**1.62**	**1.68**	**2.40**	**2.60**
Reduction site			**Li^+**	**TFEO**	**FSI^-**	**FSI^-**	**FSI^-**	**FSI^-**

For HCEs, as a result of the increase of Li salt concentration, salt anions participate in the SEI layer formation by shifting from a solvent decomposition to a salt anion decomposition/reaction. In the case of LHCE solutions, our calculations show that the decomposition of TFEO diluent can also contribute to the SEI formation when the ion pair is close to TFEO molecules located near the surface. Interestingly, XPS experiments by Zhang et al.[19] revealed the formation of a homogeneous SEI film integrated by all the anion atomic species, and C atoms that could come both from the solvent or TFEO. The CF_3 group identified in the XPS analysis was associated with TFEO decomposition. [19] In most characterization experiments, the sources of LiF are not distinguishable. However, clever experiments have shown useful to investigate this point. XPS analyses on the SEI layer formed on the Li anode surfaces in the 1 M LiFSI/ 1H,1H,5H-octafluoropentyl-1,1,2,2-tetrafluoroethyl ether (OFE) + DME were performed with OFE/DME volume ratios of 50:50 and 95:5, denoted as DME50 and DME5.[20] This experiment showed that the content of Li-F bonds significantly increased in the DME5 electrolyte, while the Li-O bond is the dominant type for the element Li in the SEI layer formed by DME50 electrolyte. To prove that TFEO molecules contribute F to a LiF layer formed on top of the Li metal anode, one can envision a test where the a non-fluorinated salt and DME as the solvent together with the fluorinated diluent constitute the electrolyte.

Finally, it is useful to reflect on the comparison between the timeframes of the dynamics obtained from first principles simulations, and those from the experimental analyses. The reaction time rate depends on the occurrence of several different (although coupled) events. For example, one can monitor the rate of the individual electrolyte decomposition reactions in contact with the pristine metal surface, or after the SEI is growing, or the rate of nucleation of the SEI products. The SEI ultrafast reactions in the order of femto- to picoseconds detected from AIMD simulations cannot be identified in most of the experiments. Thus, the value of these simulations is that they allow characterizing ultrafast reactions and competitions among them for the first 1-2nm SEI nucleation. On the other hand, the SEI products start accumulating (tens of nm) in the order of nanoseconds (detectable by the experiment and by classical MD simulations). The SEI growth after the initial ~1-2 nm will have slower decomposition rates, because the reactions will not take place directly at the pristine or partially SEI-covered electrode surface, and the electron transfer may depend on the migration of charged radical fragments through the SEI layer.[25] In summary, comparing reaction rates in this time-dependent complex reactive system is only possible when we carry out a model experiment with controlled conditions suitable to be compared with molecular simulations. Even between different experiments, the rate comparisons require a lot of care. However, each experiment or simulation provides a set of insights that corresponds to a specific timeframe. When put together, these analyses are very useful in providing the overall picture.

Conclusions

Overall, these results suggest that at the concentration used in this study, TFEO does not participate in the coordination of Li^+ directly but it can play a role because of its abundance in relation to

DME. The local coordination environment of DME -Li^+-FSI^- in the diluted electrolytes undergoes no significant change except when the complexes are close to the surface and undergo reduction reactions. When it comes to the decomposition products, because the DME molecule is a quite stable solvent, the initial SEI layer is mainly derived from the decomposition of salt anions and (probably in less proportion) of TFEO molecules. The resulting decomposed products from the reduction of LiFSI and TFEO would gradually migrate to the surface of the Li metal slab resulting in the formation of a multicomponent atomically dispersed SEI layer. The results help explaining recent experimental results[19] regarding the formation of a monolithic layer including atomic species such as F, O, N, S, from the anion decomposition. Given the large concentration of the diluent, and the role of the charged radical anion fragments on inducing further SEI growth, [25] these studies suggest that the SEI layer is dominated by atomic species from the anion decomposition and (near the surface) from the TFEO decomposition as well.

Given the complete anion reduction observed in the simulations as well as in the experiments,[19] we suggest that at the very initial stages, near the Li metal surface, a thin film constituted by atomic species mainly from the decomposition of the anion but also from TFEO molecules forms rapidly. The components of this film (in the first 1-2 nm in contact with the surface) are atomic radicals or radical anions paired with Li ions from the surface. As suggested in previous work,[25] the atomic radical anions are the ones transferring the electrons as the film grows, reducing new TFSI anions.

In addition, the simulation results offer an explanation regarding the better protection to the Li anode exerted by the LHCE-derived SEI film during many cycles as well as the reduced "pulverization" of the anode.[19] Note that the "pulverization" effect is due to the oxidation/dissolution of the Li metal in contact with the electrolyte phase. In less stable electrolytes,[27] various electrolyte components are being reduced almost simultaneously leading to fast oxidation-dissolution. Consequently, the electrode phase becomes porous and extended SEI regions form that contain nucleating structures of various components. In contrast, for the LHCE electrolyte, although the TFEO diluent also can be reduced, the simulations show that such decomposition takes place near the surface only when is induced by radical anions from the anion decomposition, otherwise TFEO is stable. Since DME is also much more stable compared to the anion, a compact SEI is formed due mainly to anion and limited TFEO decomposition. Thus, the stability of the electrolyte is the key for mitigating the oxidation/dissolution of the metal electrode with the subsequent long-term stabilization of the anode.

Acknowledgements

This material is based upon work supported by the U.S. Department of Energy's Office of Energy Efficiency and Renewable Energy (EERE), as part of the Battery 500 Consortium, Award Number DE-EE0008210 and under Contract No. DE-EE0007766 of the Advanced Battery Materials Research (BMR) Program. Supercomputer resources from the Texas A&M University High Performance Computer Center and Texas Advanced Computing Center (TACC) are gratefully acknowledged.

References

(1) Tarascon, J. M.; Armand, M. Issues and challenges facing rechargeable lithium batteries. *Nature* **2001**, *414*, 359-367.

(2) Murphy, D. W.; Christian, P. A. Solid State Electrodes for High Energy Batteries. *Science* **1979**, *205*, 651.

(3) Marom, R.; Amalraj, S. F.; Leifer, N.; Jacob, D.; Aurbach, D. A review of advanced and practical lithium battery materials. *Journal of Materials Chemistry* **2011**, *21*, 9938-9954.

(4) Aurbach, D.; Cohen, Y. The Application of Atomic Force Microscopy for the Study of Li Deposition Processes. *Journal of The Electrochemical Society* **1996**, *143*, 3525-3532.

(5) Lu, Y.; Tu, Z.; Archer, L. A. Stable lithium electrodeposition in liquid and nanoporous solid electrolytes. *Nature Materials* **2014**, *13*, 961.

(6) Lin, D.; Liu, Y.; Cui, Y. Reviving the lithium metal anode for high-energy batteries. *Nat. Nanotechnol.* **2017**, *12*, 194.

(7) Ding, F.; Xu, W.; Chen, X.; Zhang, J.; Engelhard, M. H.; Zhang, Y.; Johnson, B. R.; Crum, J. V.; Blake, T. A.; Liu, X.; Zhang, J.-G. Effects of Carbonate Solvents and Lithium Salts on Morphology and Coulombic Efficiency of Lithium Electrode. *Journal of The Electrochemical Society* **2013**, *160*, A1894-A1901.

(8) Aurbach, D.; Zinigrad, E.; Cohen, Y.; Teller, H. A short review of failure mechanisms of lithium metal and lithiated graphite anodes in liquid electrolyte solutions. *Solid State Ion.* **2002**, *148*, 405-416.

(9) Chen, S. R.; Zheng, J. M.; Mei, D. H.; Han, K. S.; Engelhard, M. H.; Zhao, W. G.; Xu, W.; Liu, J.; Zhang, J. G. High-Voltage Lithium-Metal Batteries Enabled by Localized High-Concentration Electrolytes. *Adv. Mater.* **2018**, *30*, 7.

(10) Xu, W.; Wang, J.; Ding, F.; Chen, X.; Nasybulin, E.; Zhang, Y.; Zhang, J.-G. Lithium metal anodes for rechargeable batteries. *Energy & Environmental Science* **2014**, *7*, 513-537.

(11) Foroozan, T.; Soto, F. A.; Yurkiv, V.; Sharifi-Asl, S.; Deivanayagam, R.; Huang, Z.; Rojaee, R.; Mashayek, F.; Balbuena, P. B.; Shahbazian-Yassar, R. Synergistic Effect of Graphene Oxide for Impeding the Dendritic Plating of Li. *Advanced Functional Materials* **2018**, *28*, 1705917.

(12) Zheng, J.; Lochala, J. A.; Kwok, A.; Deng, Z. D.; Xiao, J. Research Progress towards Understanding the Unique Interfaces between Concentrated Electrolytes and Electrodes for Energy Storage Applications. *Advanced Science* **2017**, *4*, 1700032.

(13) Wang, J.; Yamada, Y.; Sodeyama, K.; Chiang, C. H.; Tateyama, Y.; Yamada, A. Superconcentrated electrolytes for a high-voltage lithium-ion battery. *Nature Communications* **2016**, *7*, 12032.

(14) Qian, J.; Adams, B. D.; Zheng, J.; Xu, W.; Henderson, W. A.; Wang, J.; Bowden, M. E.; Xu, S.; Hu, J.; Zhang, J.-G. Anode-Free Rechargeable Lithium Metal Batteries. *Advanced Functional Materials* **2016**, *26*, 7094-7102.

(15) Zheng, J.; Chen, S.; Zhao, W.; Song, J.; Engelhard, M. H.; Zhang, J.-G. Extremely Stable Sodium Metal Batteries Enabled by Localized High-Concentration Electrolytes. *ACS Energy Letters* **2018**, *3*, 315-321.

(16) Adams, B. D.; Zheng, J.; Ren, X.; Xu, W.; Zhang, J.-G. Accurate Determination of Coulombic Efficiency for Lithium Metal Anodes and Lithium Metal Batteries. *Advanced Energy Materials* **2018**, *8*, 1702097.

(17) Chen, S.; Zheng, J.; Mei, D.; Han, K. S.; Engelhard, M. H.; Zhao, W.; Xu, W.; Liu, J.; Zhang, J.-G. High-Voltage Lithium-Metal Batteries Enabled by Localized High-Concentration Electrolytes. *Advanced Materials* **2018**, *30*, 1706102.

(18) Park, M. S.; Ma, S. B.; Lee, D. J.; Im, D.; Doo, S.-G.; Yamamoto, O. A Highly Reversible Lithium Metal Anode. *Scientific Reports* **2014**, *4*, 3815.

(19) Cao, X.; Ren, X.; Zou, L.; Engelhard, M. H.; Huang, W.; Wang, H.; Matthews, B. E.; Lee, H.; Niu, C.; Arey, B. W.; Cui, Y.; Wang, C.; Xiao, J.; Liu, J.; Xu, W.; Zhang, J.-G. Monolithic solid–electrolyte interphases formed in fluorinated orthoformate-based electrolytes minimize Li depletion and pulverization. *Nature Energy* **2019**, *4*, 796-805.

(20) Zheng, J.; Ji, G.; Fan, X.; Chen, J.; Li, Q.; Wang, H.; Yang, Y.; DeMella, K. C.; Raghavan, S. R.; Wang, C. High-Fluorinated Electrolytes for Li–S Batteries. *Advanced Energy Materials* **2019**, *9*, 1803774.

(21) Hagos, T. T.; Thirumalraj, B.; Huang, C.-J.; Abrha, L. H.; Hagos, T. M.; Berhe, G. B.; Bezabh, H. K.; Cherng, J.; Chiu, S.-F.; Su, W.-N.; Hwang, B.-J. Locally Concentrated LiPF6 in a Carbonate-Based Electrolyte with Fluoroethylene Carbonate as a Diluent for Anode-Free Lithium Metal Batteries. *ACS Appl. Mater. Interfaces* **2019**, *11*, 9955-9963.

(22) Shi, S. Q.; Gao, J.; Liu, Y.; Zhao, Y.; Wu, Q.; Ju, W. W.; Ouyang, C. Y.; Xiao, R. J. Multi-scale computation methods: Their applications in lithium-ion battery research and development. *Chin. Phys. B* **2016**, *25*, 018212.

(23) Wang, A. P.; Kadam, S.; Li, H.; Shi, S. Q.; Qi, Y. Review on modeling of the anode solid electrolyte interphase (SEI) for lithium-ion batteries. *Npj Computational Materials* **2018**, *4*, 15.

(24) Horstmann, B.; Single, F.; Latz, A. Review on multi-scale models of solid-electrolyte interphase formation. *Curr. Opin. Electrochem.* **2019**, *13*, 61-69.

(25) Soto, F. A.; Ma, Y.; Martinez-DeLaHoz, J. M.; Seminario, J. M.; Balbuena, P. B. Formation and Growth Mechanisms of Solid-Electrolyte Interphase Layers in Rechargeable Batteries *Chem. Mater.* **2015**, *27*, 7990-8000.

(26) Leung, K.; Budzien, J. L. Ab initio molecular dynamics simulations of the initial stages of solid-electrolyte interphase formation on lithium ion battery graphitic anodes. *Phys. Chem. Chem. Phys.* **2010**, *12*, 6583-6586.

(27) Bertolini, S.; Balbuena, P. B. Buildup of Solid Electrolyte Interphase on Lithium-Metal Anode: Reactive Molecular Dynamics Study. *J. Phys. Chem. C* **2018**, *in press*.

(28) Borodin, O.; Bedrov, D. Interfacial Structure and Dynamics of the Lithium Alkyl Dicarbonate SEI Components in Contact with the Lithium Battery Electrolyte. *J. Phys. Chem. C* **2014**, *118*, 18362-18371.

(29) Galvez-Aranda, D. E.; Ponce, V.; Seminario, J. M. Molecular dynamics simulations of the first charge of a Li-ion—Si-anode nanobattery. *Journal of Molecular Modeling* **2017**, *23*, 120.

(30) Ponce, V.; Galvez-Aranda, D. E.; Seminario, J. M. Analysis of a Li-Ion Nanobattery with Graphite Anode Using Molecular Dynamics Simulations. *J. Phys. Chem. C* **2017**, *121*, 12959-12971.

(31) Kresse, G.; Furthmuller, J. Efficiency of ab-initio total energy calculations for metals and semiconductors using a plane-wave basis set. *Comput. Mater. Sci.* **1996**, *6*, 15-50.

(32) Kresse, G.; Hafner, J. Ab initio molecular dynamics for liquid metals. *Physical Review B* **1993**, *47*, 558-561.

(33) Blöchl, P. E. Projector augmented-wave method. *Physical Review B* **1994**, *50*, 17953-17979.

(34) Henkelman, G.; Arnaldsson, A.; Jónsson, H. A fast and robust algorithm for Bader decomposition of charge density. *Computational Materials Science* **2006**, *36*, 354-360.

(35) Sanville, E.; Kenny, S. D.; Smith, R.; Henkelman, G. Improved grid-based algorithm for Bader charge allocation. *Journal of Computational Chemistry* **2007**, *28*, 899-908.

(36) Camacho-Forero, L. E.; Smith, T. W.; Bertolini, S.; Balbuena, P. B. Reactivity at the Lithium–Metal Anode Surface of Lithium–Sulfur Batteries. *The Journal of Physical Chemistry C* **2015**, *119*, 26828-26839.

(37) Camacho-Forero, L. E.; Smith, T. W.; Balbuena, P. B. Effects of High and Low Salt Concentration in Electrolytes at Lithium–Metal Anode Surfaces. *The Journal of Physical Chemistry C* **2017**, *121*, 182-194.

(38) Stephens, P. J.; Devlin, F. J.; Chabalowski, C. F.; Frisch, M. J. Ab Initio Calculation of Vibrational Absorption and Circular Dichroism Spectra Using Density Functional Force Fields. *The Journal of Physical Chemistry* **1994**, *98*, 11623-11627.

(39) Wodrich, M. D.; Corminboeuf, C.; Schreiner, P. R.; Fokin, A. A.; Schleyer, P. v. R. How Accurate Are DFT Treatments of Organic Energies? *Organic Letters* **2007**, *9*, 1851-1854.

(40) Sun, H.; Mumby, S. J.; Maple, J. R.; Hagler, A. T. An *Ab Initio* CFF93 All-Atom Force Field for Polycarbonates. *J. Am. Chem. Soc.* **1994**, *116*, 2978-2987.

(41) Canongia Lopes, J. N.; Shimizu, K.; Pádua, A. A. H.; Umebayashi, Y.; Fukuda, S.; Fujii, K.; Ishiguro, S.-i. Potential Energy Landscape of Bis(fluorosulfonyl)amide. *J. Phys. Chem. B* **2008**, *112*, 9449-9455.

(42) Ponce, V.; Galvez-Aranda, D. E.; Seminario, J. M. Analysis of a Li-Ion Nanobattery with Graphite Anode Using Molecular Dynamics Simulations. *J. Phys. Chem. C* **2017**, *121*, 12959-12971.

(43) Mennucci, B. Polarizable continuum model. *Wiley Interdisciplinary Reviews: Computational Molecular Science* **2012**, *2*, 386-404.

(44) Yamada, Y.; Wang, J.; Ko, S.; Watanabe, E.; Yamada, A. Advances and issues in developing salt-concentrated battery electrolytes. *Nature Energy* **2019**, *4*, 269-280.

(45) Camacho-Forero, L. E.; Balbuena, P. B. Elucidating electrolyte decomposition under electron-rich environments at the lithium-metal anode. *Phys. Chem. Chem. Phys.* **2017**, *19*, 30861-30873.

Table of Contents Graphic